Journal of Science and Technology in Civil Engineering, HUCE, 2025, 19 (2): 145–158

WAVE-STRUCTURE INTERACTIONS OF A FLOATING FPSO-SHAPED BODY

Mai Cao Tri[a,*]

[a]*Faculty of Coastal and Offshore Engineering, Hanoi University of Civil Engineering, 55 Giai Phong road, Hai Ba Trung district, Hanoi, Vietnam*

Article history:
Received 22/4/2025, Revised 05/6/2025, Accepted 13/6/2025

Abstract

This research investigates the wave scatter field surrounding floating structure via the Floating Production Storage and Off-loading (FPSO) model with a validation of experimental data collected at the Ocean Basin in University of Plymouth's COAST Laboratory. The study explores the effects of wave steepness on wave-structure interactions. As focusing on wave groups created by using NewWave with a JONSWAP spectrum, experiments were utilized in various tests. A phase-inversion technique was applied to separate the linear and higher-harmonic components of the free-surface elevation around the FPSO, as well as the mooring line force and the model's motion response. The findings illustrate the floating model significantly reduced linear harmonic that scattered waves in a comparison to the fixed model. In contrast, second-harmonic scattered waves increased substantially near the bow and alongside the floating model. Moreover, higher-harmonic scattered waves developed with an increasing of wave steepness. Similarly, the higher harmonics of mooring line force, heave, and pitch motions also increased as wave steepness intensified.

Keywords: physical model; non-linear waves; diffraction waves; FPSO; springing; ringing.

https://doi.org/10.31814/stce.huce2025-19(2)-11

1. Introduction

Wave-induced forces at integer harmonics of the primary wave frequency can trigger high-frequency resonant responses in both floating offshore structures (such as floating wind turbines, FPSOs and other platforms) and bottom-fixed structures (like gravity-based structures). The effects of nonlinear wave-wave and wave-structure interactions can lead to a nonlinear transfer of energy to higher-harmonic structural responses. As a result, the incident waves with spectral energy at the peak frequency (f_p) may induce structural vibrations at multiples of the peak frequency ($2f_p, 3f_p, 4f_p$, and so on). These higher-harmonic responses lead to pronounced nonlinear phenomena known as springing (occurring at double the wave frequency) and ringing (at triple the wave frequency), as described by Mercier [1]. Springing is primarily driven by second-order excitation at double the frequency, while ringing in gravity-based and tension leg platforms results from higher-order (third- and fourth-order) frequencies, causing transient elastic responses.

Floating Production Storage and Off-loading (FPSO) vessels are essential for offshore oil and gas production, serving as key infrastructure for processing and storage. As exploration moves into deeper waters, understanding wave interactions with FPSOs in these conditions is essential, with physical model testing remaining a key method. Past studies have explored wave-FPSO interactions, including wave scattering [2–5] and FPSO behavior in long- and short-crested seas [6]. Zang et al. [2] investigated second-order wave diffraction at the bow of a simplified FPSO, identifying a second-order bound harmonic upstream of the bow, followed by radiated free waves distinct from

*Corresponding author. *E-mail address:* trimc@huce.edu.vn (Tri, M. C.)

the incoming wave group, but no notable third-order harmonic effects. In one study by Siddorn [3], numerical simulations confirmed a significant second-order diffracted wave field but found no third-harmonic contributions at the bow or upstream. However, third-order diffraction was observed to the sides and diagonally downstream from the FPSO's stern.

Fitzgerald et al. [7] explored higher harmonic diffracted wave fields around a surface-piercing column under a focused wave group, employing NewWave theory [8]. This study tested a series of wave-structure interaction modeling for a focused wave group (with $kA = 0.1$, where k is the wavenumber linked to the spectral peak energy period, and A is the linear harmonic's total amplitude) interacting with a 0.25 m diameter cylinder, using a fully non-linear higher-order BEM potential flow model. The simulations revealed second and third harmonics in the total and scattered wave fields both upstream and downstream of the model. Moreover, this study applied the phase-based harmonic separation method [7] to break down the local wave field.

Furthermore, Mai et al. [4] examined wave-structure interactions for fixed FPSO-shaped bodies of varying lengths. The findings showed that the linear harmonic grows as the model length decreases, while non-linear harmonics remain comparable across the three tested lengths, with the second and third-harmonics peaking for the medium-length model. Additionally, the non-linear scattered waves intensify with greater wave steepness.

In this study, physical model tests were conducted with a floating FPSO model, subjected to waves of varying steepness and incident waves from a 0-degree angle (head-on). The study examines the scattered wave field around the model, the mooring line forces, and the model's motion response. Harmonic components of the scattered wave were isolated using phase-inversion and frequency filtering techniques. The linear, second, third, and fourth harmonics of the kinematic and dynamic quantities' evolution are analyzed and discussed.

2. Methodology

2.1. Floating Experiments

The experiment took place in the Ocean Basin at Plymouth University's COAST Lab, measuring 35 m long and 15.5 m wide, with a maximum water depth of 2.93 m. The floating FPSO models, constructed from aluminum at approximately 1:100 scale, was designed as a rectangular box with semicircular cylinders at the bow and stern. The model had a height and width of 0.3 m, a length of 1.2 m (see Fig. 1), and a draft of 0.15 m.

The input waves consisted of focused wave groups created using the NewWave methodology [8] with a JONSWAP spectrum ($\gamma = 3.3$) focused at the FPSO model's bow. Local wave steepness ranged from 0.13 to 0.17, with an incident wave angle of 0°. The total linear wave amplitude varies from 0.069 m to 0.089 m and the peak wave period of 1.44 s. Wave scattering around the FPSO and wave run-up on the model was captured by 24 wave gauges (see Fig. 2) at a 128 Hz sampling frequency. This paper analyzes and presents data only for local waves scattered at wave gauges WG7, WG10, and WG11 (at the focused location). Additionally, a Qualisys system tracked the six degrees of freedom (6DOF) motions of the model during floating tests. Qualisys system is a 3D motion capture system that uses infrared cameras to track the position and motion of physical models with high precision. In this study, it was used to monitor the real-time movement of the floating FPSO model. Finally, a tension load cell, anchored to the basin floor, was used to measure the tension force of the single mooring line (see Fig. 3). This load cell measured the tensile force in the mooring line. The load cell was connected in-line with the mooring rope, and the measured data was used to analyze time-varying tension forces. A single taut mooring was chosen for the floating FPSO test in this study to simplify the experimental setup, reduce costs and focus on wave scattering for comparision

with the fixed model. It is noted that using a single mooring line may affect the yaw motion of the model and it is not applicable in the sea. The mooring line consists of a Dyneema® rope (spring constant, $k \approx 35$ N/mm) connected in series with a linear spring ($k = 0.066$ N/mm) that allows for the mooring's extension. The spring's length ranges from a minimum of 435 mm to a maximum of 635 mm.

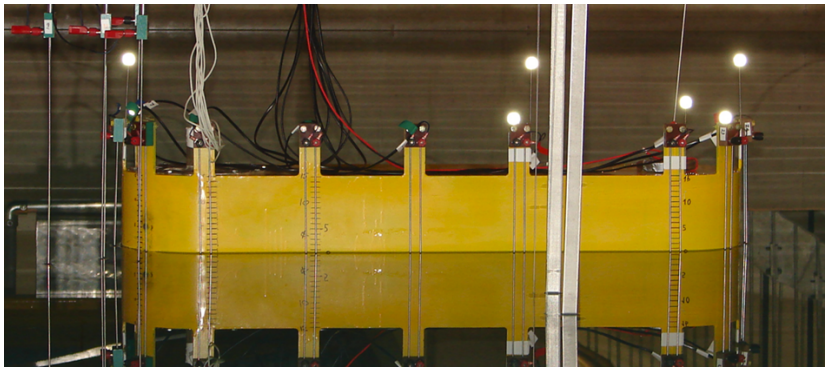

Figure 1. The tested floating FPSO model in the Ocean Basin

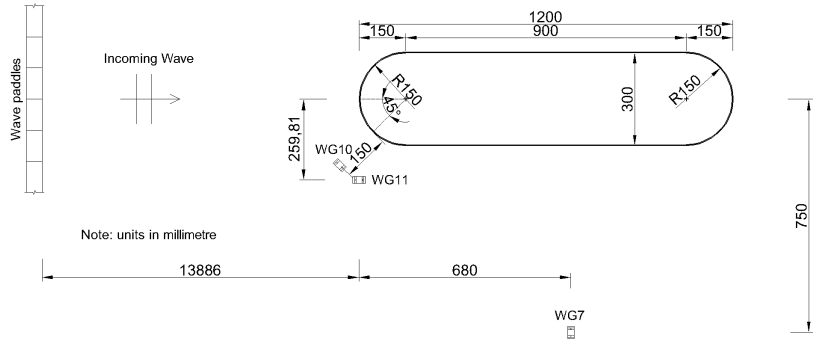

Figure 2. Wave gauge arrangement around the tested model

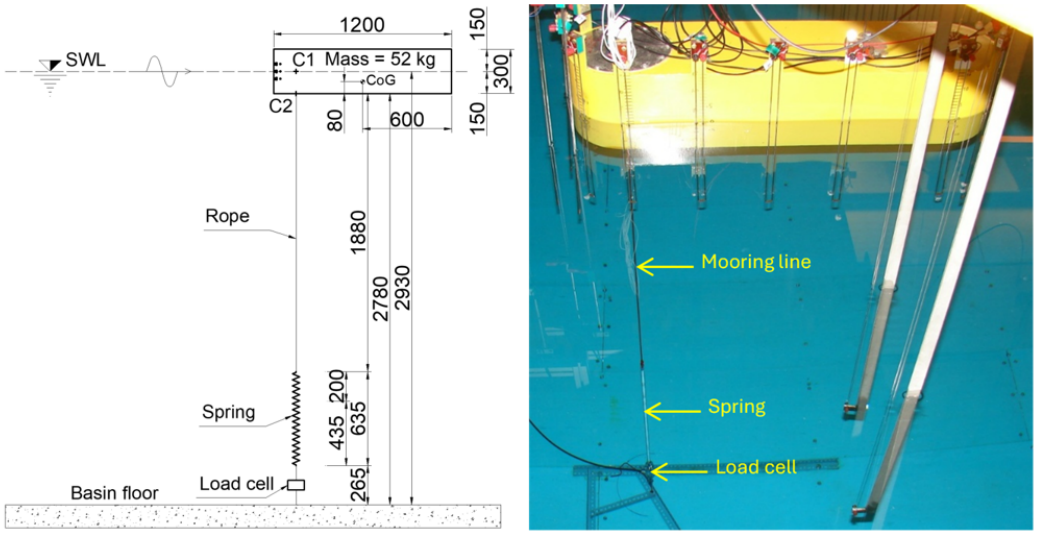

Figure 3. Single mooring line system of the floating FPSO model

2.2. *Phase-based harmonic separation method*

The phase-inversion methodology [9] is employed to isolate higher-harmonic components of the free-surface elevation. This method has been employed in previous research [2–4, 7, 10–12]. From time histories of kinematic quantities (free-surface elevation) or dynamic quantities (wave force), odd and even harmonic components can be extracted. Two incident wave groups with identical amplitudes and frequencies but opposite phases, i.e., 0° (crest-focused wave) and 180° (trough-focused wave), are used. Individual harmonics, such as linear and third-order or second- and fourth-order, can then be separated using frequency filtering. The scattered wave field can be derived by subtracting the undisturbed incident wave from the wave measured in the presence of the model, as described by Mai et al. [4].

Fig. 4 shows the time histories of the free-surface elevation, η^0 and η^{180}, at the focus location (wave gauge WG11). The vertical axis denotes the dimensionless free-surface elevation (η/A), where η is the free-surface elevation, and A is the linear amplitude at the focus location and time. The horizontal axis shows the time scale, with the focus time at $t = 0$ s. The focused wave groups in Fig. 4 have a spectral peak period $T_p = 1.44$ s and a total linear amplitude A of 0.089 m, resulting in a wave steepness of $kA = 0.17$, where k is the wavenumber corresponding to T_p. Applying the phase-inversion technique for η^0 and η^{180} in Fig. 4, the linear and the first three higher-order sum harmonic components were derived and displayed in Fig. 5 for their amplitude spectra and in Fig. 6 for their time histories.

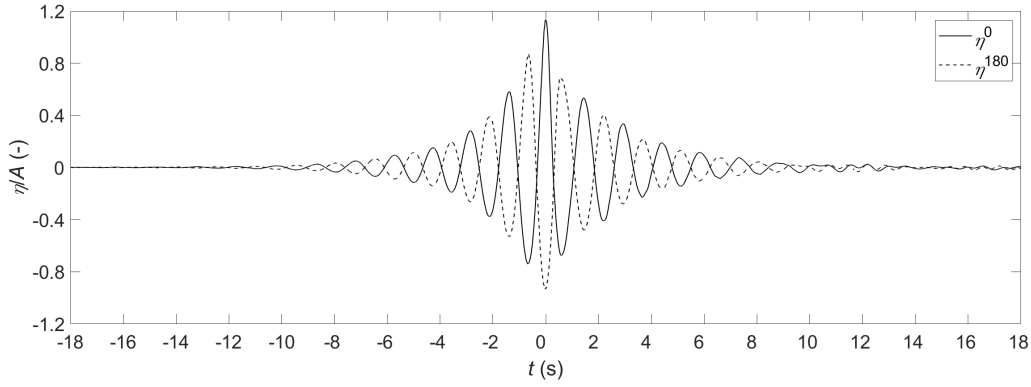

Figure 4. The tested wave profiles at the focus point WG11 (no model, $kA = 0.17$)

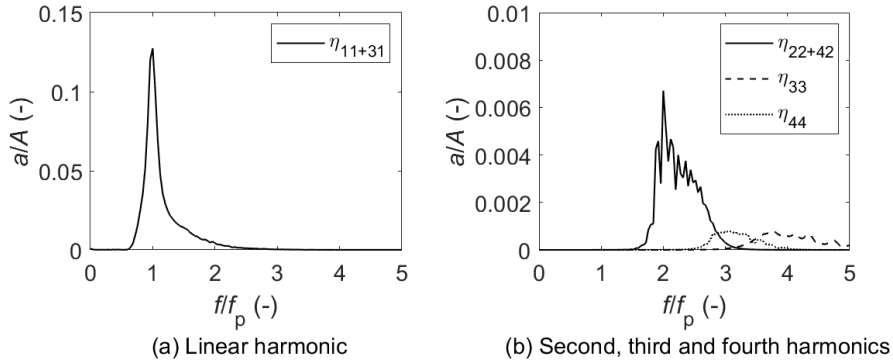

Figure 5. Amplitude spectra of the extracted harmonics at the focus point WG11 (no model, $kA = 0.17$)

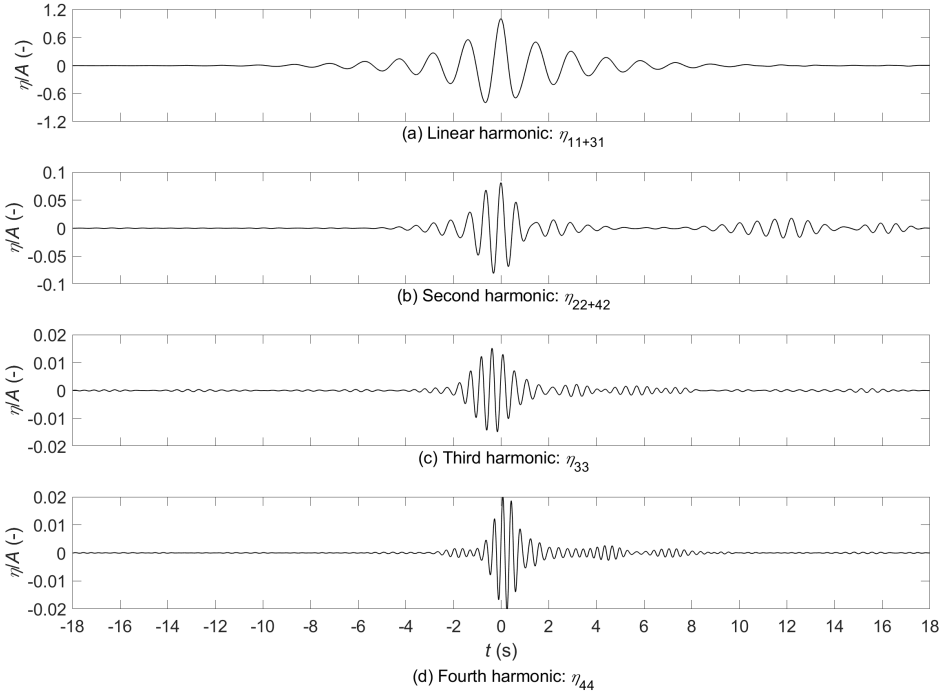

Figure 6. Time series for the separated components at the focus point WG11 (no model, $kA = 0.17$)

3. Results

This section illustrates waves scatter around the floating FPSO model. Lately, effects of wave steepness on the mooring line force and motion response of the floating FPSO is investigated. The experiment utilized a single taut mooring line, which generated force over the duration of one wave group as the moored model oscillated. Tests were conducted using crest-focused (η^0) and trough-focused (η^{180}) wave groups for the FPSO. The single mooring line system layout is depicted in Fig. 3. Two wave gauge positions were studied: one near the bow (WG10) and one at the side (WG7) of the FPSO, as presented in Fig. 4.

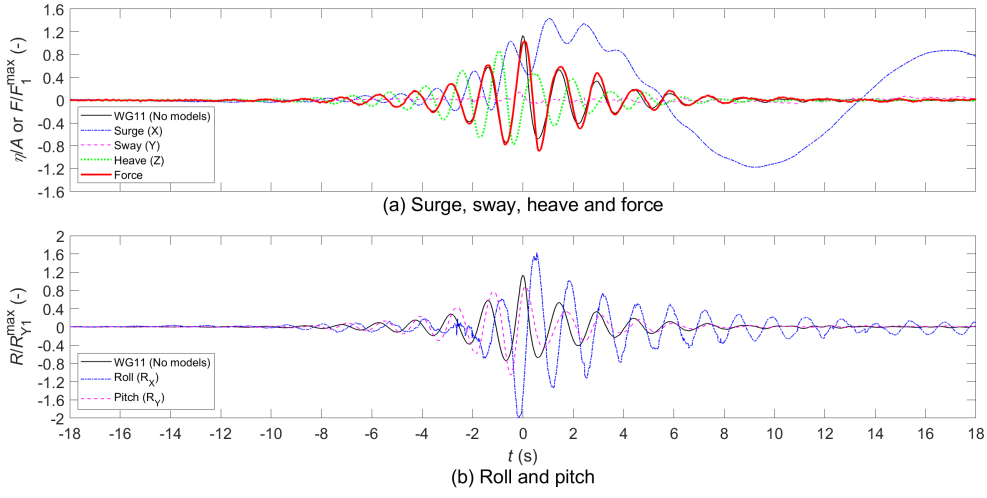

Figure 7. Typical time series of the mooring line force and motion response of the floating FPSO model ($kA = 0.17$, Phase $\theta = 0°$)

Fig. 7 and Fig. 8 show typical time series of the mooring line force and motion response of the floating FPSO model at a wave steepness of $kA = 0.17$. The undisturbed water elevation at the focal point (WG11) is shown in Fig. 7(a) and Fig. 8(a). The vertical axis represents dimensionless values, with $F_1^{\max}$ and $R_{Y1}^{\max}$ indicating the total linear amplitude of the mooring line force and pitch motion, respectively. Regrettably, the yaw motion measurement signal was lost.

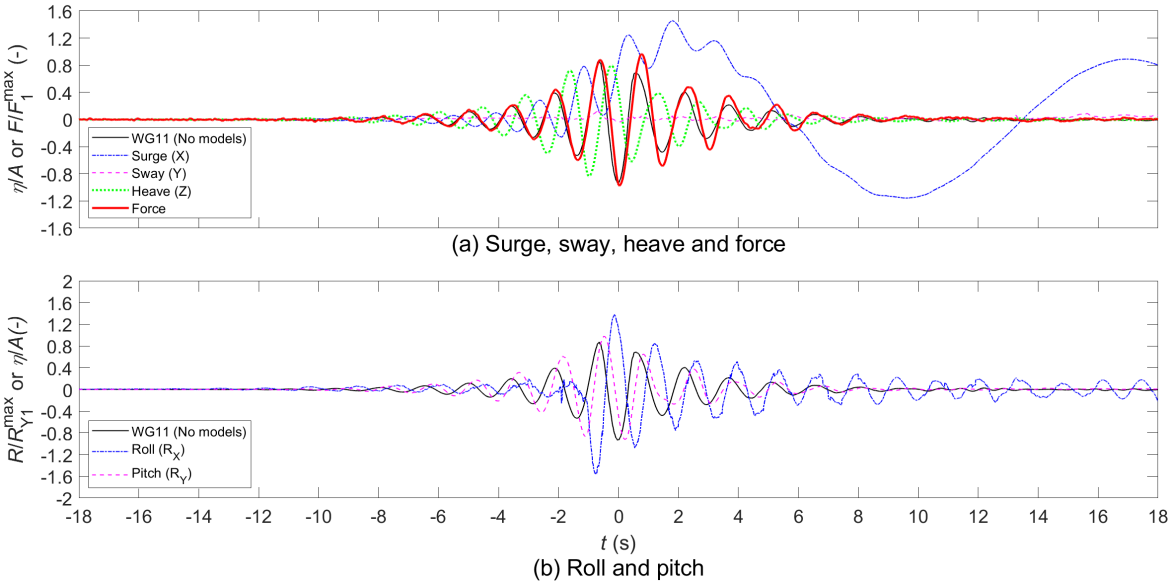

Figure 8. Typical time series of the mooring line force and motion response of the floating FPSO model ($kA = 0.17$, Phase $\theta = 180°$)

3.1. Wave scattering around the fixed and floating FPSO

Water elevations at two locations (WG7 and WG10) are analysed to assess the impact of the floating model on the scattered wave field, with a comparison to the fixed model from Mai et al. [4], where the fixed FPSO model has the same dimensions as the floating FPSO model in this study. Results are shown for the steepest wave ($kA = 0.17$) tested with the floating FPSO model.

a. Near the bow

Using the phase-inversion separation technique outlined in Section 2.2, the linear and higher harmonic components (η_{11}, η_{22}, η_{33}, η_{44}) of the water surface elevation are extracted from wave gauge WG10 at the bow of the model. The amplitude spectra corresponding to the time histories of these components are depicted in Fig. 9. Comparing spectra with and without the models reveals a significant increase in spectral amplitude due to wave-model interactions, except for the linear harmonic (η_{11}), which is reduced for the floating model compared to the fixed model and the no-model case (Fig. 9(a)). Notably, the floating model enhances the amplitude spectra of the second and fourth harmonics (η_{22} & η_{44}) more strongly than the fixed model (Figs. 9(b), (d)). The third harmonic (η_{33}) amplitude spectra are similar for both fixed and floating models (Fig. 9(c)).

The time histories of these harmonic components, obtained via inverse FFT of the filtered amplitude spectra, are shown in Fig. 10 for cases with and without models. Wave scattering by the model significantly amplifies the free-surface elevation of the linear and higher harmonics. For the linear component, the floating model produces a lower crest and deeper trough than the fixed model (Fig. 10(a)). Conversely, the second harmonic exhibits the highest crest and lowest trough with the

floating model (Fig. 10(b)), while the third and fourth harmonics are comparable for both models (Figs. 10(c), (d)).

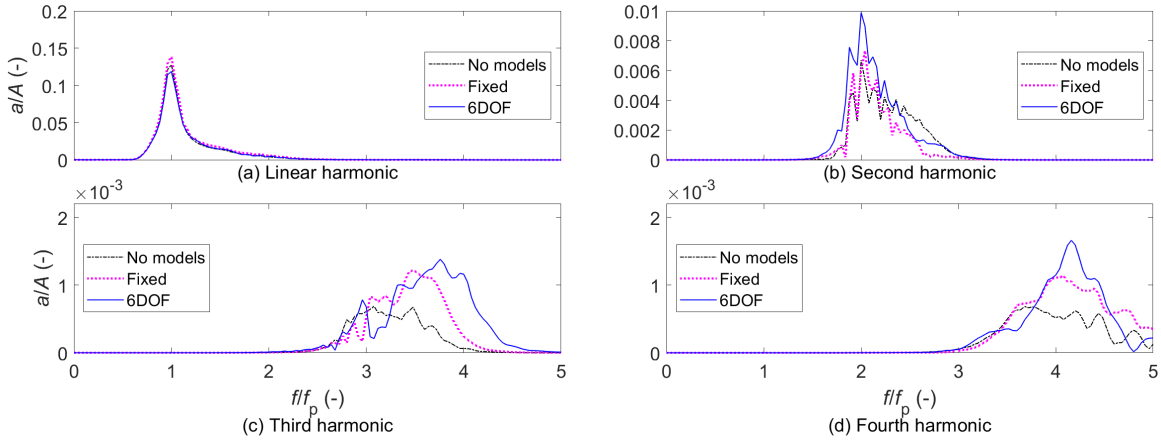

Figure 9. Amplitude spectra of the extracted harmonics near the bow of the fixed and floating FPSO models for $kA = 0.17$ (WG10)

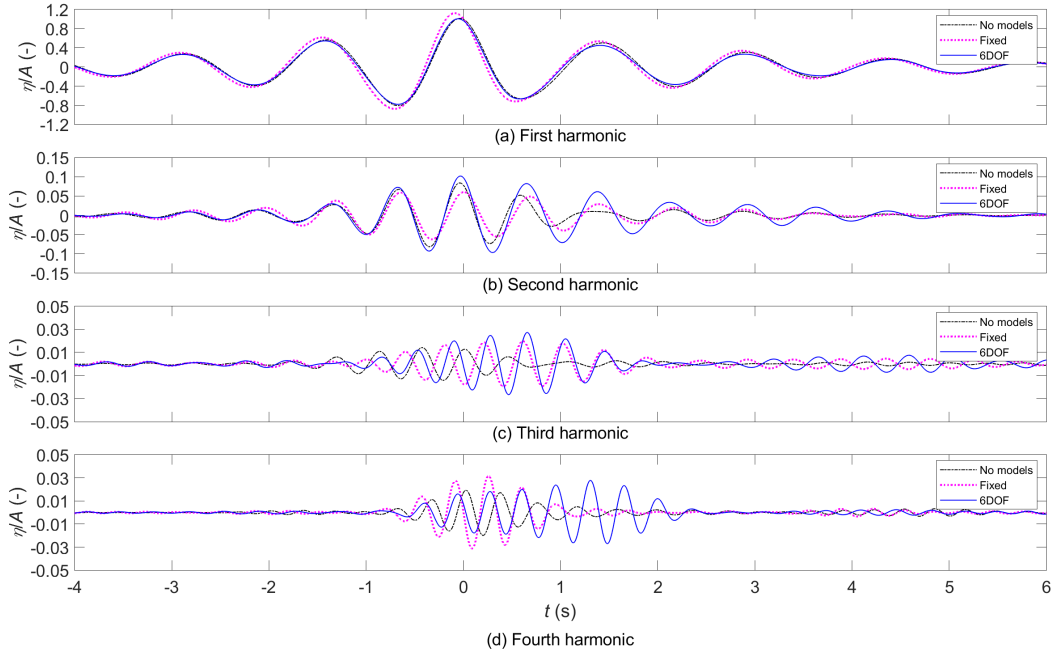

Figure 10. Time series of the separated wave components near the bow of the fixed and floating FPSO models for $kA = 0.17$ (WG10)

Scattered wave data, derived by subtracting time histories with and without models, are presented in Fig. 11. The scattered waves' linear, third, and fourth harmonics are most pronounced with the fixed model (Figs. 11(a), (c), (d)), while the second harmonic is strongest with the floating model (Fig. 11(b)). Figs. 11(c), (d) also reveal a secondary pulse in the third and fourth harmonics of the scattered wave field at approximately $t = +3.5$ s, potentially causing an additional load cycle on the structure.

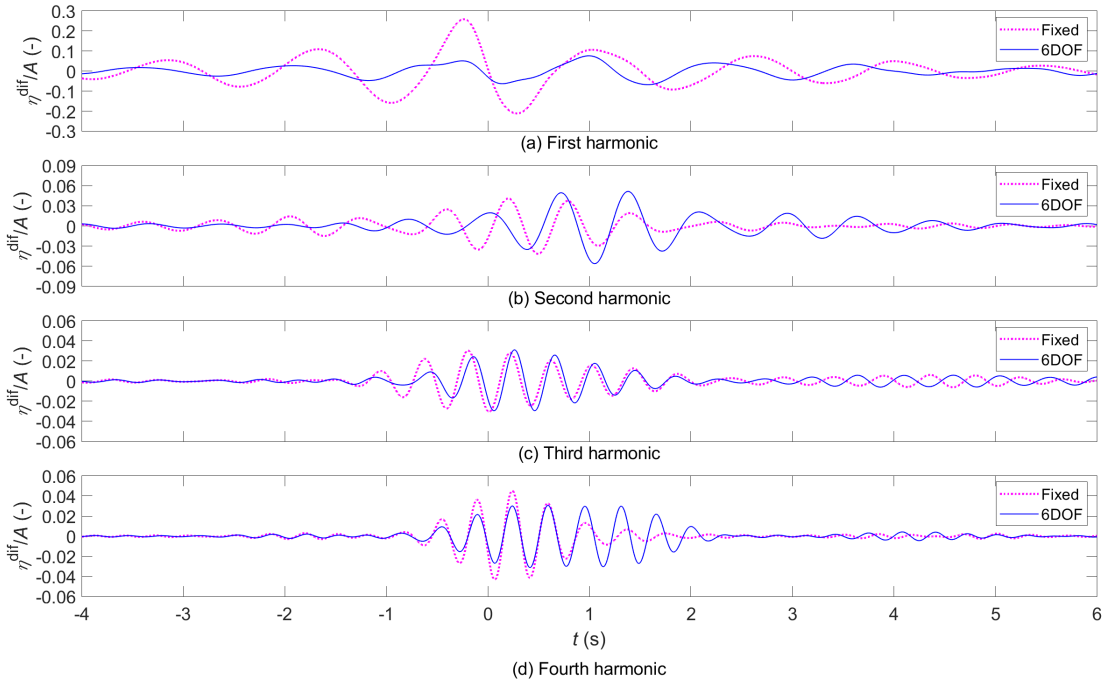

Figure 11. Time series of the scattered waves near the bow of the fixed and floating FPSO models for $kA = 0.17$ (WG10)

b. Alongside

Wave scattering alongside the fixed and floating models is analysed using wave gauge WG7, as shown in Fig. 2. The amplitude spectra of the linear and higher harmonic components are displayed in Fig. 12. Consistent with observations near the bow, the linear component's amplitude spectrum is lower for the floating model than for the fixed model or without a model (Fig. 12(a)). The second and third harmonics show the highest amplitudes with the floating model (Figs. 12(b), (c)), while the fourth harmonic spectra are similar but exhibit some variability for both models (Fig. 12(d)), likely due to the sensitivity of the harmonic extraction process to time alignment accuracy, particularly for the fourth harmonic.

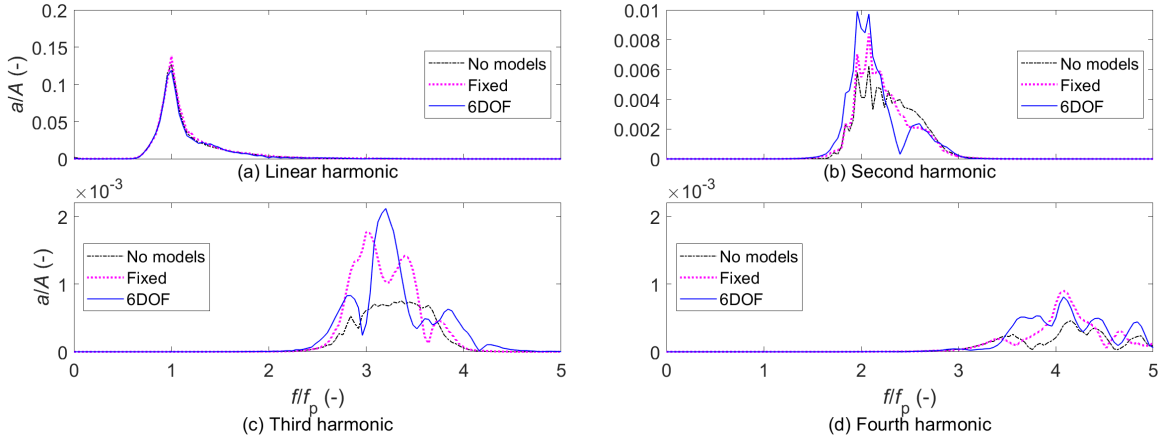

Figure 12. Amplitude spectra of the extracted harmonics alongside the fixed and floating FPSO models for $kA = 0.17$ (WG7)

The time histories of the scattered waves' linear and higher harmonic components alongside the models are shown in Fig. 13. The wave-structure interaction has a weaker effect on the linear component for the floating model compared to the fixed model (Fig. 13(a)), but it is significantly stronger for the second harmonic (Fig. 13(b)). The third and fourth harmonic free-surface elevations are nearly identical for both models (Figs. 13(c), (d)).

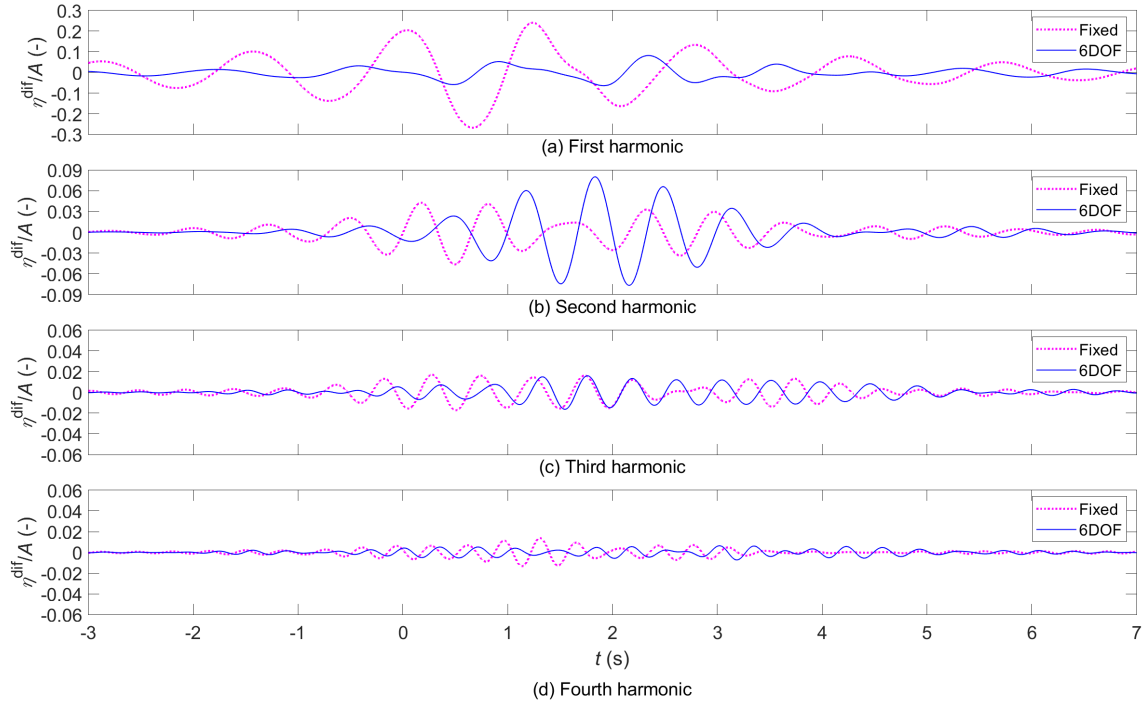

Figure 13. Time series of the scattered waves alongside the fixed and floating FPSO models for $kA = 0.17$ (WG7)

3.2. *Effect of wave steepness on wave scattering and mooring line force*

The influence of wave steepness on wave scattering, mooring line force, and motion response is evaluated for the floating FPSO model (Fig. 3) using focused wave groups with steepness values of $kA = 0.13$ and 0.17 at two locations: near the bow (WG10) and alongside (WG7). The analysis includes the mooring line force and the heave and pitch motion responses.

Using the phase-inversion separation method with frequency filtering (Section 2.2), the amplitude spectra of the linear and higher harmonic components are analyzed. Following Mai et al. [4] for the fixed model, this section focuses on the higher harmonics to study the effect of wave steepness on the floating model's wave-structure interaction. The amplitude spectra of the second, third, and fourth harmonics are shown in Fig. 14 and Fig. 15 for WG10 and WG7, respectively. As expected, the higher harmonics' amplitude spectra increase with wave steepness from $kA = 0.13$ (solid line) to $kA = 0.17$ (dashed line), consistent with the fixed model results. The second harmonic's amplitude spectrum near the bow is notably higher than alongside for $kA = 0.13$, but they are comparable for $kA = 0.17$ (Fig. 14(a), Fig. 15(a)). The third and fourth harmonics show slight variations between locations (Figs. 14(b), (c), Figs. 15(b), (c)), with wave steepness most significantly affecting the third and fourth harmonics near the bow, where some amplitudes nearly double (Figs. 14(b), (c)).

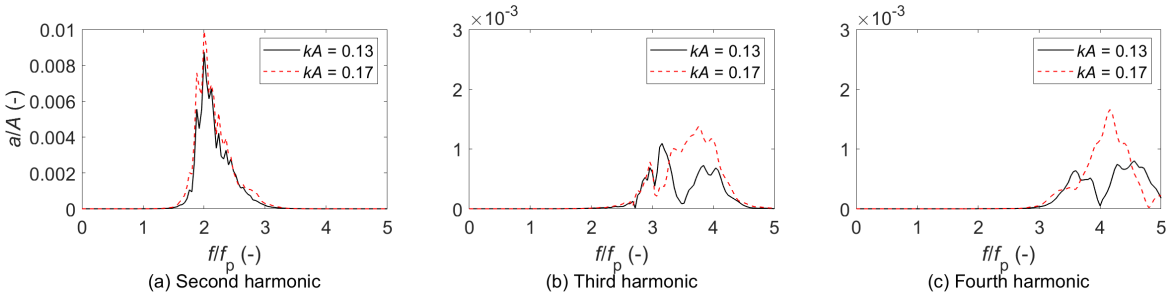

Figure 14. Amplitude spectra of the extracted harmonics near the bow of the floating FPSO model (WG10)

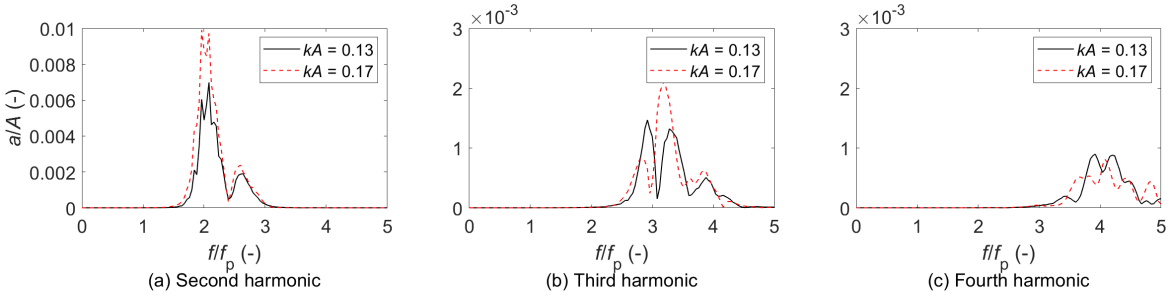

Figure 15. Amplitude spectra of the extracted harmonics alongside the floating FPSO model (WG7)

The filtered time histories of the higher harmonics of the scattered wave fields at the bow and alongside the floating FPSO model are presented in Fig. 16 and Fig. 17, respectively. Near the bow, the second harmonic shows slight amplification (Fig. 16(a)), while the third and fourth harmonics are significantly affected by wave steepness (Figs. 16(b), (c)). Alongside, the second harmonic is notably influenced by wave steepness (Fig. 17(a)), but the third harmonic remains unaffected (Fig. 17(b)), and the fourth harmonic's amplitude decreases with increasing steepness (Fig. 17(c)). Consistent with Mai et al. [4], the fourth harmonic near the bow is significantly higher than alongside (Figs. 16(c), 17(c)), attributed to geometric spreading and gauge positioning.

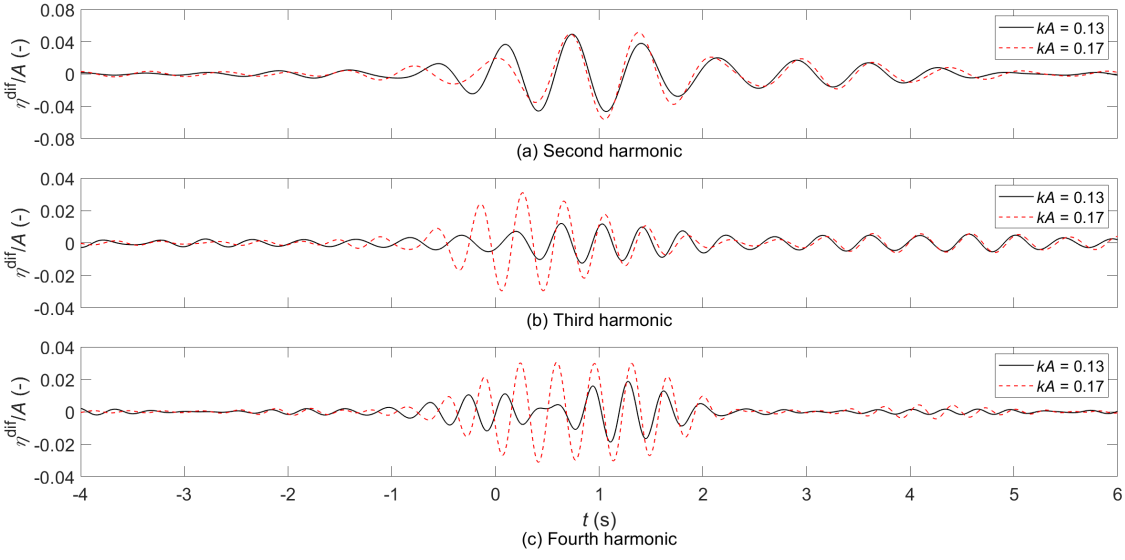

Figure 16. Time series of the scattered components near the bow of the floating FPSO model (WG10)

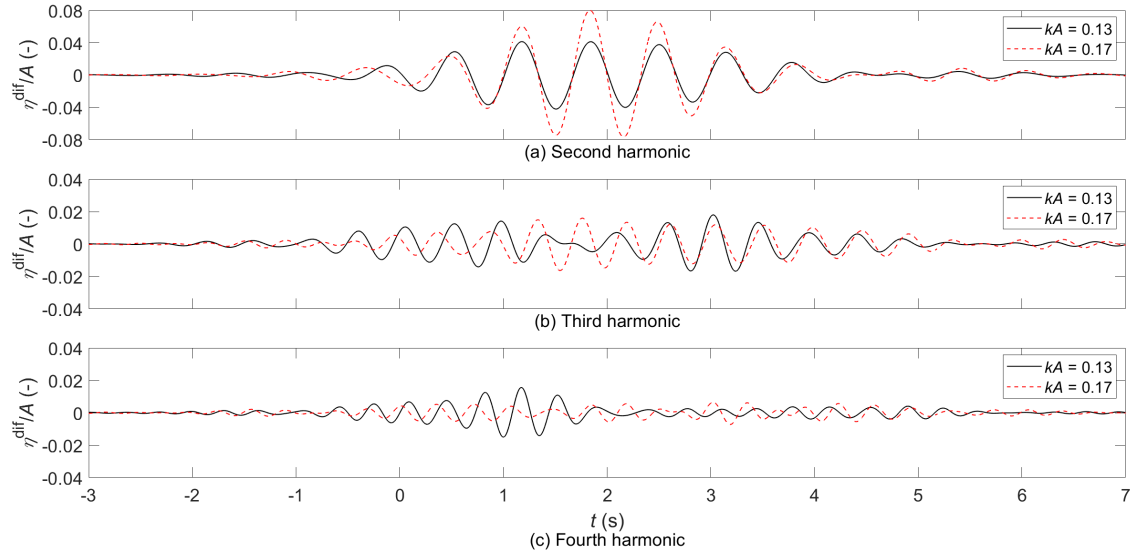

Figure 17. Time series of the scattered components alongside the floating FPSO model (WG7)

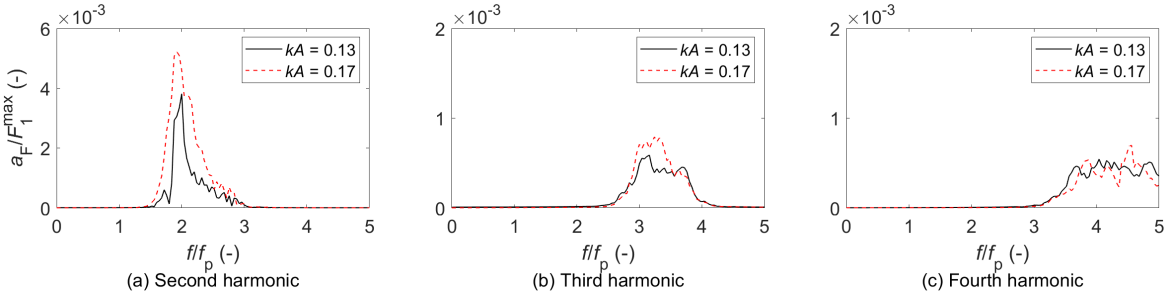

Figure 18. Amplitude spectra of the extracted harmonics of the mooring line force of the floating FPSO model

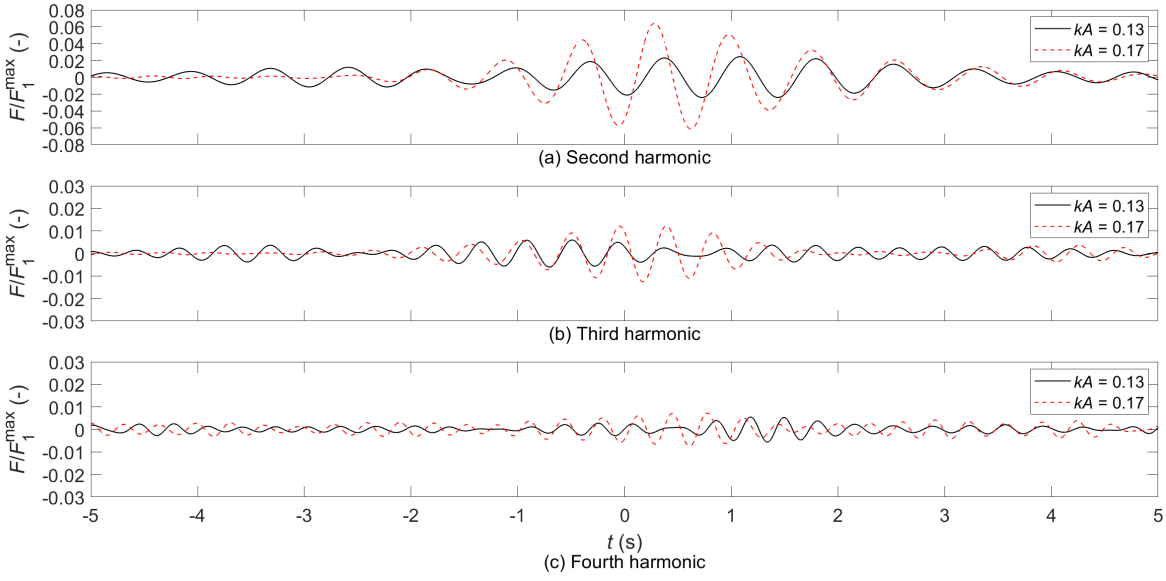

Figure 19. Time series of the separated components of the mooring line force of the floating FPSO model

The linear and higher harmonic components of the mooring line force, heave, and pitch motions are extracted using the phase-inversion method. The amplitude spectra and time histories of the mooring line force's higher harmonics are shown in Fig. 18 and Fig. 19, respectively, with the vertical axis representing dimensionless force ($F_1^{\max}$ as the total linear amplitude). The second and third harmonics' amplitude spectra increase significantly with wave steepness from $kA = 0.13$ to 0.17 (Figs. 18(a), (b)), but the fourth harmonic remains nearly unchanged (Fig. 18(c)). The time histories confirm this, showing the second and third harmonics' amplitudes increase by three and two times, respectively, with higher steepness, while the fourth harmonic is unaffected (Fig. 19).

The amplitude spectra of the heave and pitch motions are shown in Fig. 20 and Fig. 22, respectively. As with the mooring line force, the second and third harmonics of both motions increase significantly with wave steepness (Figs. 20(a), (b) and Figs. 22(a), (b)), with the fourth harmonic showing a slight increase (Figs. 20(c) and 22(c)). The corresponding time histories (Figs. 21(a)–(c) and Figs. 23(a)–(c)) confirm the pronounced effect of wave steepness on the motion response, consistent with the mooring line force findings in Figs. 18 and 19.

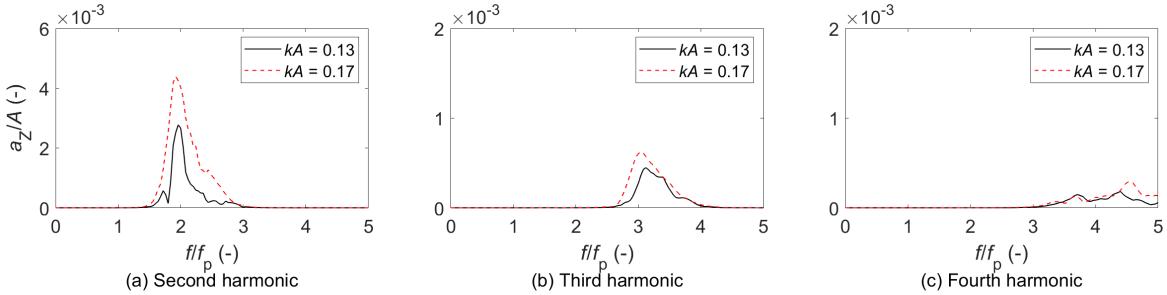

Figure 20. Amplitude spectra of the extracted harmonics of the heave motion of the floating FPSO model

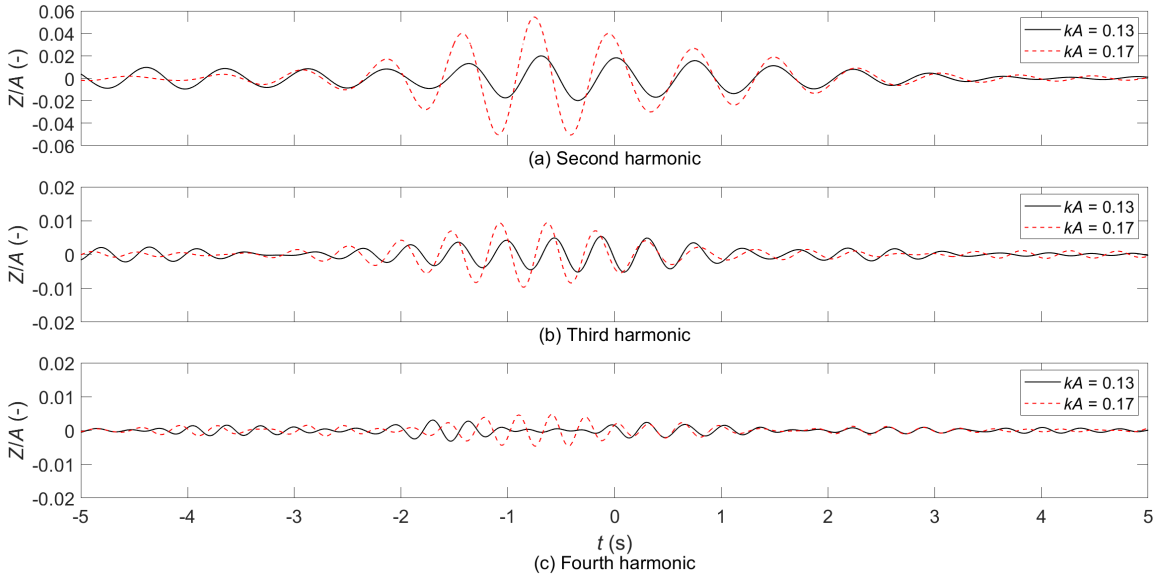

Figure 21. Time series of the separated components of the heave motion of the floating FPSO model

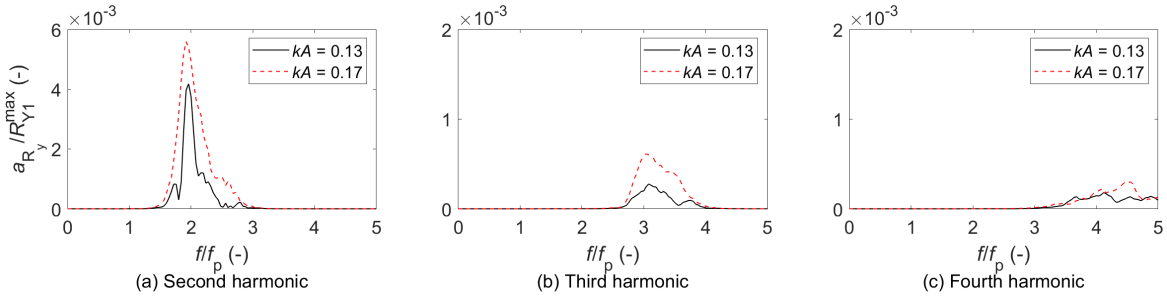

Figure 22. Amplitude spectra of the extracted harmonics of the pitch motion of the floating FPSO model

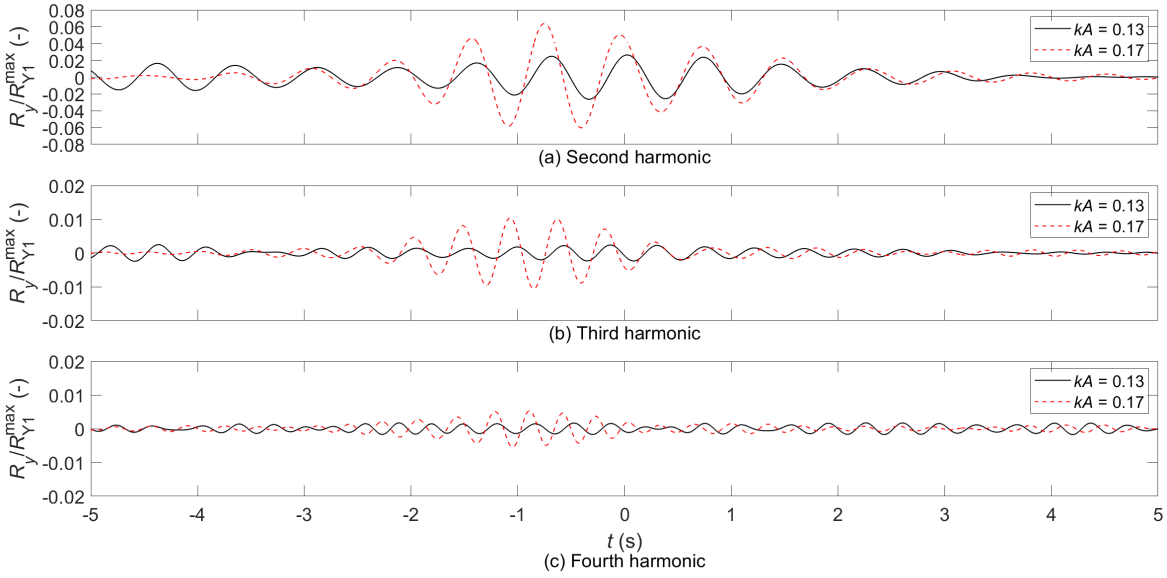

Figure 23. Time series of the separated components of the pitch motion of the floating FPSO model

4. Conclusions

This study presents an experimental investigation into wave scattering around a floating FPSO model, examining the force on a single mooring line and the nodel's motions. Tests were conducted in the Ocean Basin at the University of Plymouth with water depth of 2.93 m, using various focused wave groups. It is found that, compared to the fixed model [4], the floating model significantly reduces linear harmonic scattered waves but markedly increases second harmonic scattered waves both upstream and alongside. Consistent with the fixed model, higher harmonic scattered waves increase with greater wave steepness. Additionally, increased wave steepness amplifies the higher harmonics of the mooring line force, heave, and pitch motions. Higher order components (the second, third and four harmonics) of water surface elevation, mooring line force and model' motions should be considered for design and stability assessment of FPSO mooring systems in preliminary design stages.

Acknowledgments

This study was a part of the FROTH (Fundamentals and Reliability of Offshore sTructure Hydrodynamics) project supported by the Engineering and Physical Science Research Council (EPSRC Grant EP/J012866/1). The FROTH project was being led by Plymouth University, and the collaborative partners include Oxford University, University of Bath, City University London and the Manch-

ester Metropolitan University. The author gratefully acknowledges the financial support provided by EPSRC and useful discussions with Prof. Deborah Greaves, Prof. Alison Raby, and the project partners.

References

[1] Mercier, J. A. (1982). Evolution of tension leg platform technology. In *Proceedings of the 3rd International Conference on the Behaviour of Offshore Structures*, Massachusetts Institute of Technology, Cambridge, MA.

[2] Zang, J., Gibson, R., Taylor, P. H., Eatock Taylor, R., Swan, C. (2006). Second order wave diffraction around a fixed ship-shaped body in unidirectional steep waves. *Journal of Offshore Mechanics and Arctic Engineering*, 128(2):89–99.

[3] Siddorn, P. D. (2012). *Efficient numerical modelling of wave-structure interaction*. DPhil. University of Oxford.

[4] Mai, T., Greaves, D., Raby, A., Taylor, P. H. (2016). Physical modelling of wave scattering around fixed FPSO-shaped bodies. *Applied Ocean Research*, 61:115–129.

[5] Ransley, E., Yan, S., Brown, S. A., Mai, T., Graham, D., Ma, Q., Musiedlak, P.-H., Engsig-Karup, A. P., Eskilsson, C., Li, Q., Wang, J., Xie, Z., Venkatachalam, S., Stoesser, T., Zhuang, Y., Li, Q., Wan, D., Chen, G., Chen, H., Qian, L., Ma, Z., Mingham, C., Causon, D., Gatin, I., Jasak, H., Vukcevic, V., Downie, S., Higuera, P., Buldakov, E., Stagonas, D., Chen, Q., Zang, J., Greaves, D. (2019). A Blind Comparative Study of Focused Wave Interactions with a Fixed FPSO-like Structure (CCP-WSI Blind Test Series 1). *International Journal of Offshore and Polar Engineering*, 29(2):113–127.

[6] HR Wallingford Ltd (2002). *FPSO response in long and short crested seas*. HSE OT Report 2002/018.

[7] Fitzgerald, C. J., Taylor, P. H., Taylor, R. E., Grice, J., Zang, J. (2014). Phase manipulation and the harmonic components of ringing forces on a surface-piercing column. *Proceedings of the Royal Society A: Mathematical, Physical and Engineering Sciences*, 470(2168):20130847.

[8] Tromans, P. S., Anaturk, A. R., Hagemeijer, P. (1991). A new model for the kinematics of large ocean waves - application as a design wave. In *Proceedings of the 1st International Offshore and Polar Engineering Conference*, Edinburgh, U.K., 64–71.

[9] Baldock, T. E., Swan, C., Taylor, P. H. (1996). A Laboratory Study of Non-linear Surface Waves on Water. *Philosophical Transactions of the Royal Society of London. Series A: Mathematical, Physical and Engineering Sciences*, 354(1707):649–676.

[10] Hunt, A., Taylor, P., Borthwick, A., Stansby, P., Feng, T. (2004). Kinematics of a Focused Wave Group on a Plane Beach: Physical Modeling in the UK Coastal Research Facility. In *Coastal Structures 2003*, American Society of Civil Engineers, 740–750.

[11] Borthwick, A. G. L., Hunt, A. C., Feng, T., Taylor, P. H., Stansby, P. K. (2006). Flow kinematics of focused wave groups on a plane beach in the U.K. Coastal Research Facility. *Coastal Engineering*, 53 (12):1033–1044.

[12] Hann, M., Greaves, D., Raby, A. (2014). A new set of focused wave linear combinations to extract non-linear wave harmonics. In *Twenty-ninth International Workshop on Water Waves and Floating Bodies*, Osaka, Japan, 61–64.